NANO LETTERS

2005
Vol. 5, No. 4
697−703

Penetrating the Oxide Barrier in Situ and Separating Freestanding Porous Anodic Alumina Films in One Step

Mingliang Tian,*[†,‡] Shengyong Xu,[†,‡] Jinguo Wang,[†] Nitesh Kumar,[†,‡] Eric Wertz,[‡] Qi Li,[†,‡] Paul M. Campbell,[||] Moses H. W. Chan,[†,‡] and Thomas E. Mallouk*[†,§]

Materials Research Institute and Center for Nanoscale Science, Department of Physics, and Department of Chemistry, Pennsylvania State University, University Park, Pennsylvania 16802, and Naval Research Laboratory, Washington, D.C. 20375

Received January 18, 2005; Revised Manuscript Received February 21, 2005

ABSTRACT

A simple method for penetrating the barrier layer of an anodic aluminum oxide (AAO) film and for detaching the AAO film from residual Al foil was developed by reversing the bias voltage in situ after the anodization process is completed. With this technique, we have been able to obtain large pieces of free-standing AAO membranes with regular pore sizes of sub-10 nm. By combining Ar ion milling and wetting enhancement processes, Au nanowires were grown in the sub-10 nm pores of the AAO films. Further scaling down of the pore size and extension to the deposition of nanowires and nanotubes of materials other than Au should be possible by further optimizing this procedure.

Porous membranes with pore diameters from nanometers to micrometers have been used extensively as templates for the fabrications of nanowires with a variety of compositions and complex structures,[1−16] carbon nanotubes,[17] and metal and alumina nanotubule membranes.[18,19] Relative to other porous media, such as polycarbonate membranes, well-fabricated anodic alumina oxide (AAO) membranes possess a much higher pore density—up to about 10^{11}pores/cm^2—and a narrower distribution of pore diameters. The diameter and density of the pores are controllable by varying the anodization voltage of high-purity aluminum foil or film with a specific electrolyte, for examples, phosphoric acid (H_3PO_4),[20] sulfuric acid (H_2SO_4),[21] or oxalic acid ($H_2C_2O_4$).[22] The pore channels of a good AAO membrane are mostly parallel to each other and perpendicular to the surface of the membrane. The length of the pore channels is also adjustable from submicrometer to tens of micrometers, and the AAO membrane is especially suited for use at higher temperatures. Therefore, AAO membranes have been widely used as templates for electronic and electrochemical devices or in sensing and catalytic applications.

However, two major problems are encountered in the fabrication of AAO membranes. First, as shown schematically in Figure 1, after the anodization process, there is always an alumina barrier layer between the bottom of the pore and the unanodized base aluminum that serves as the electrochemical anode. This insulating barrier layer usually has a thickness of 10−100 nm. It can thus block direct electrical and chemical contact between the substances in the pore channels and the base conducting substrate in applications such as dc electrodeposition of nanowires and

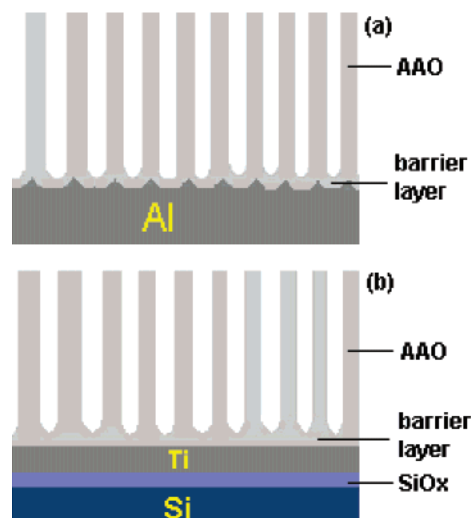

Figure 1. Schematic of the cross section of porous anodic alumina (AAO) films grown on (a) an aluminum foil substrate and (b) a Ti/Si$_x$O/Si wafer.

* To whom correspondence should be addressed. E-mail: mut1@psu.edu (Tian) or tom@chem.spu.edu (Mallouk).
[†] Materials Research Institute and Center for Nanoscale Science, Pennsylvania State University.
[‡] Department of Physics, Pennsylvania State University.
[§] Department of Chemistry, Pennsylvania State University.
[||] Naval Research Laboratory.

10.1021/nl0501112 CCC: $30.25 © 2005 American Chemical Society
Published on Web 03/03/2005

field-emission devices. Second, the anodized AAO layer is firmly attached to the base aluminum, making it difficult to obtain free-standing AAO membranes for some applications.

A common practice to overcome these problems is to etch away the base aluminum substrate with saturated $HgCl_2$ and then etch away the exposed barrier layer with ~6 wt % H_3PO_4. In another approach, after the AAO film is formed the bias voltage is progressively stepped down in 5% decrements, causing perforation of the barrier layer.[20] This is followed by further chemical etching at the AAO/aluminum interface with an acid (H_2SO_4 or H_3PO_4) that detaches the AAO film from the base aluminum foil. Because both approaches induce isotropic chemical etching of the alumina film, they both inevitably enlarge the pore size. With the progressive miniaturization of electronic devices, there is now a need to study the electrical and structural properties in systems of ultrathin nanowires. In this field, large pieces of free-standing AAO films with pore sizes as small as a few nanometers could play an important role if an approach to penetrate the barrier layer without significantly enlarging the original pore size of the anodized AAO film can be developed.

However, because the free-standing AAO films are fragile when their thickness is less than 10 μm, it is of great interest to develop methods to fabricate thin AAO film on rigid Si substrates for device design,[23] thermoelectric,[24,25] and field emitter[26] devices by depositing nanowire or carbon nanotube arrays directly onto these substrates. To realize these devices, the oxide barrier layer of the AAO films must be penetrated in situ. Rabin et al.[27] investigated AAO films on Si wafers with a metallic Ti adhesion layer and reported that the oxide barrier layer could be removed by cathodically biasing the film in KCl solution for a few minutes. Thinning of the alumina barrier layer was thought to involve a local increase of the pH value over 8. However, the Ti adhesion layer was also oxidized when the Al layer was fully anodized with 0.04 M oxalic acid or 20 vol % H_2SO_4.[27] Electrodeposition in an AAO film on a Si wafer without removing the insulating barrier layer has also been reported,[17,26,28] where the growth of NWs was achieved by using an ac method or by utilizing the tiny conduction paths that may be embedded in the alumina barrier layer. In that case, the higher barrier resistance greatly adds to the impedance of nanodevices and thus restricts their applications, such as in field emitters.

In this paper, we demonstrate that penetrating the oxide barrier layer of an AAO film and detaching the film from the base aluminum can be realized in situ in one step by reversing the polarity of the voltage immediately after the completion of the anodization process. With this technique, we have routinely obtained large-area free-standing AAO membranes with an average pore diameter below 10 nm.

Two types of AAO films were prepared by using a standard anodization procedure from (a) 99.999% pure Al foils (Aldrich, 100 mm × 100 mm × 1 mm) and (b) electron-beam-evaporated Al/Ti double layers on 4 in. thermally oxidized (100) Si wafers (Al/Ti/SiO_x/Si), respectively, as shown schematically in Figure 1. Before anodization, the as-purchased Al foils were mechanically polished and annealed at 350 °C for 6 h. The Al foils were then electrochemically polished for 10 min in an electrolyte composed of 60 vol % H_3PO_4 and 40 vol % H_2SO_4 at 75 °C, with an electrical current density of 125 mA/cm^2. The surface of the well-polished Al foil is shiny and mirrorlike. This process is extremely important in making large pieces of high-quality AAO films. For Al/Ti/SiO_x/Si samples, because the Al films had a smooth surface, they were directly anodized without any polishing. Dilute sulfuric acid (3 vol % H_2SO_4) was chosen as the electrolyte for the anodization process at 0−3 °C. Because the dissolution rate of the AAO film in dilute sulfuric acid is negligible near 0 °C, this enables us to obtain small-pore AAO films at a relatively high voltage, 16−18 V, without causing excessive current flow and heat evolution. A pure Pb or Pt plate was used as the electrochemical cathode in the experiments.

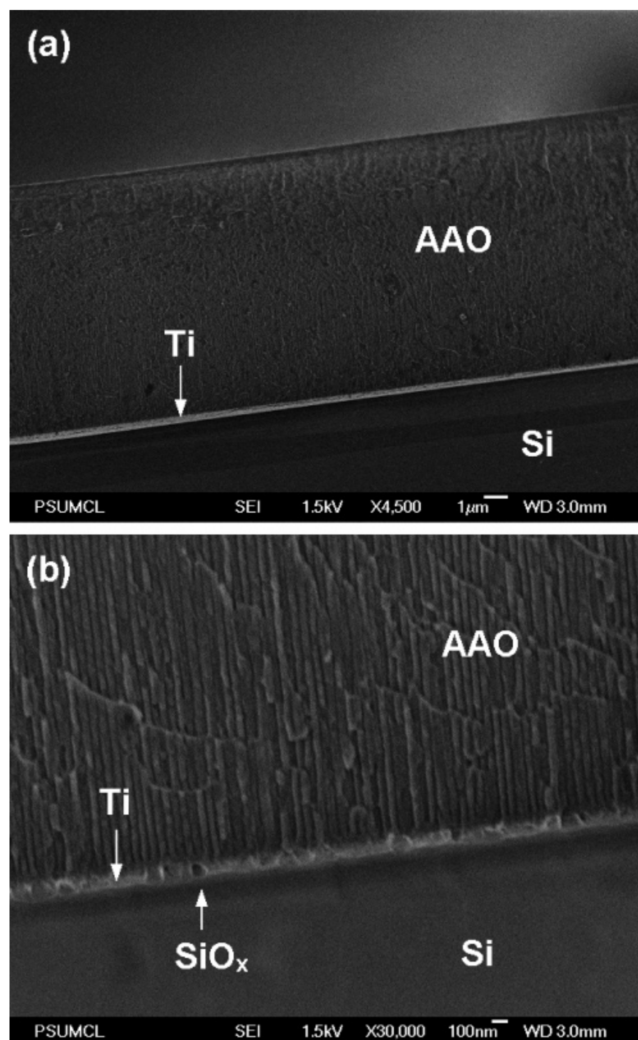

Figure 2. FESEM images of the cross section of an as-anodized AAO/Ti/Si_xO/Si sample, which was anodized at 18 V and 0−3 °C in 3 vol % H_2SO_4, showing the uniform Ti layer and continuous AAO/Ti interface: (a) low-magnification image; (b) high-magnification image. The original 9 μm Al film was made by electron-beam evaporation under a base pressure of 1×10^{-6} Torr. The deposition rates were 20−25 Å/s for the Al layer and 5 Å/s for the Ti adhesion layer.

Figure 2a shows a field-emission scanning electron microscope (FESEM) image of the cross section of an

original 9-μm-thick as-anodized AAO film on a SiO_x/Si substrate with a Ti adhesion layer, anodized under a voltage of 18.0 V at 0−3 °C. Both the AAO and Ti films show uniform thickness throughout the imaged area. There are no voids or cracks between the AAO and Ti film in the close up of the AAO/Ti interface of the same sample, as shown in Figure 2b. Instead, an oxide barrier layer with a thickness of 20−30 nm is clearly seen between the bottom of the pores and the Ti layer. The pore diameter of the AAO film is about 15 nm, and the spacing between two nonintersecting pores ranges from 20 to 30 nm. The thickness of the thermally oxidized SiO_x layer and the Ti adhesion layer is approximately 200 nm, indicated by the arrows.

To penetrate in situ the oxide barrier layer shown in Figure 2, a reversed-bias voltage (−3.5 to −5 V) was applied immediately to the sample in the same electrolyte after the aluminum film was completely anodized. When bubbles (H_2) were observed coming from the pores at the AAO film surface, the bias voltage was reduced until no more bubbles were observed. This reversing process took a few minutes. When copious bubbles uniformly spread out from the AAO film surface, the bias voltage was adjusted to zero. To observe the effects of the reversed-bias process on the barrier layer of the AAO film, the cross section of an AAO/Ti/SiO_x/Si sample after the reversed bias (i.e., −3.5 V for 10 min in the same electrolyte at 0−3 °C) was examined by FESEM, as shown in Figure 3a and b. The oxide barrier layer that was seen in Figure 2 is completely removed, and the pores are thus open to the Ti layer. Voids and cracks are developed along the interface between the Ti layer and the AAO film by the reversed bias because the bottom oxide barrier layer was etched away as a result of the over-etching process. By exactly controlling the etching time and the magnitude of the negatively biased voltage, one can selectively penetrate the bottom oxide barrier of the pores vertically but not destroy the oxide walls transversely between the neighboring pores at the bottom. The initial magnitude of the reversed voltage and the total time required to penetrate the barrier layer depend on the thickness of the barrier layer. Generally, both increase with an increase in the anodization voltage.

The results indicate a selective etching process at negative bias. As mentioned above, Rabin et al.[27] suggested that the oxide barrier layer could be removed by cathodically biasing the film in neutral saturated KCl solution. The thinning mechanism of the AAO barrier was thought to involve a local increase of the pH value over 8 at the cathode. To understand the thinning mechanism in our case with acidic solution, we carried out a dye (Phloxine B) fluorescence experiment[29] to monitor the variations of the pH value at the electrochemical cathode under a bias voltage. Initially, we prepared a series of solutions with different pH values ranging from 1 to 8 and verified that the fluorescence of the 0.025 mM dye under UV excitation is bright yellow at pH ≥3, below which the fluorescence is reddish. Then we tested our 3 vol % H_2SO_4 electrolyte with the 0.025 mM dye. Because the pH value was below 1 at zero bias, the sample always showed a reddish fluorescence. After applying a bias voltage of −2 to −4 V, we still did not detect any yellowish fluorescence near the cathode. This result indicates that the pH value at the cathode must be lower than 3 in 3 vol % H_2SO_4 solution even at a cathodic bias voltage. Any mechanisms involving a local increase in the pH value over 8 can be ruled out by this experiment, and this is consistent with the high initial concentration of acid. We postulate that the reverse bias may actually result in an increase in the local concentration of H^+ ions at the barrier layer. Prior to the penetration of the barrier layer, the H^+ ions can migrate to the bottom of the pores under the electric field. This locally higher concentration of H^+ ions promotes the dissolution of the oxide barrier layer and thus opens the pores. Once the barrier layer is penetrated, the pH value is expected to increase, corresponding to the consumption of the H^+ ions at the cathode. The dissolution reaction can be expressed as $Al_2O_3(s) + 6H^+(aq) \rightarrow 2Al^{3+}(aq) + 3H_2O(l)$. After dissolving the barrier layer, the H^+ ions in the electrolyte migrate to the Ti cathode, where they leave the electrolysis cell in the form of H_2 gas (i.e., $2H^+(aq) + 2e^- \rightarrow H_2(g)$. Because the sulfuric acid electrolyte is more dilute (3 vol % H_2SO_4)

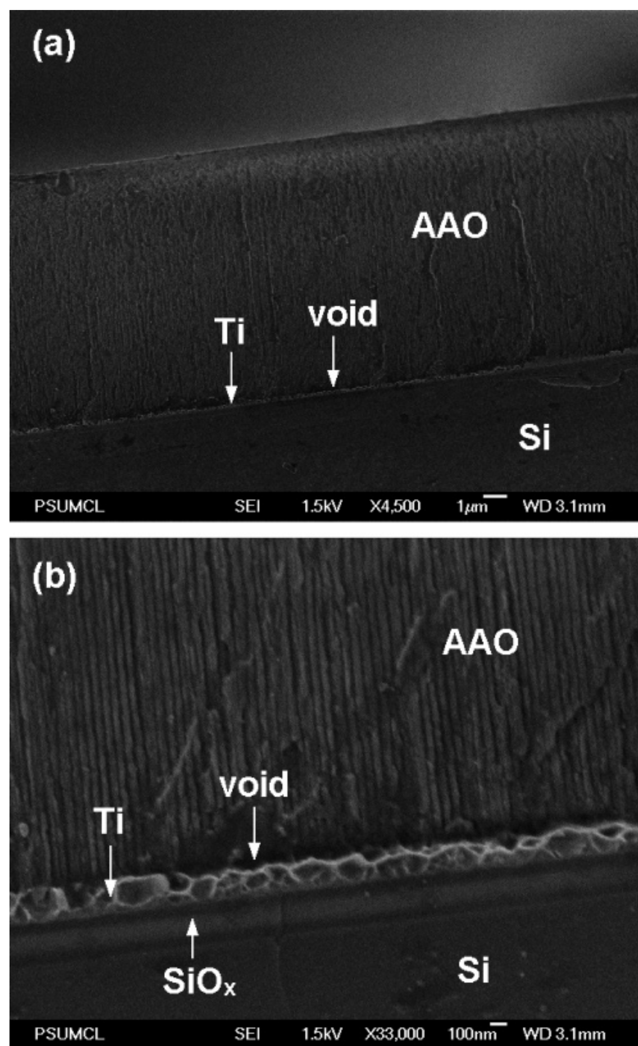

Figure 3. FESEM images of the cross section of the same AAO/Ti/Si_xO/Si sample shown in Figure 2, after the reversed-bias process at −3.5 V for 10 min, showing penetration of the oxide barrier layer and cracks or voids at the AAO/Ti interface: (a) low-magnification image; (b) high-magnification image.

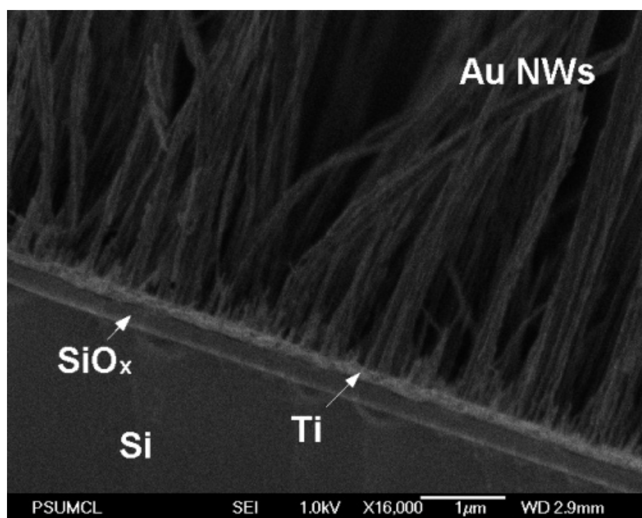

Figure 4. FESEM image of high-density Au nanowire array or bundles grown with an AAO film on a Ti/SiO_x/Si substrate, where the AAO film was completely dissolved with 5 M NaOH solution.

than that used by Dresselhaus et al.,[27] the Ti adhesion layer remains metallic. No column-shaped TiO_x structures are observed in Figure 3, and thus Au nanowires can be directly electrodeposited into the pores of the AAO film by using a dc voltage with the Ti layer working as the cathode.

Figure 4 shows an FESEM image of Au nanowires grown with the AAO film on Ti/SiO_x/Si, where the AAO film was completely dissolved by using 5 M NaOH solution. The nanowires were made with a commercial Au bath (Orotemp, Technic Inc) at a dc voltage of −2.5 V.[5] The successful growth of the high-density nanowire array or bundles with dc voltage confirms that the Ti layer is conducting and the pores in the AAO film are open to the Ti layer. There are no significant problems in fabricating nanowires into the AAO film if the size of the voids or the thickness of the cracks is less than 50 nm. (In this case, the AAO film remains on the substrate.) The small voids or cracks can be quickly filled by Au growth in the first minute, and then the Au is forced to grow into the nanopores. The performance of this kind of nanostructure with high aspect ratio (length/diameter ≈ 400−900) nanowires should not be very different from that of nanostructures grown from AAO without voids or cracks. This is because the deposited Au in filling the voids or cracks is highly conducting and remains in good contact with the Ti layer.

However, if the reverse-bias etching time is long enough, larger voids and cracks will be formed between the AAO and the Ti layer. Once these voids and cracks connect to each other, the AAO film will lift off from the substrate, and thus the growth of nanowires becomes impossible. Using this method, we were also able to detach AAO films from the residual Al foils. We have routinely obtained large free-standing AAO membranes (over 10 cm × 5 cm) with average pore diameters from 30 nm down to sub-10 nm by this technique. Figure 5a shows an FESEM image of the bottom surface of a free-standing AAO film made at 16 V and 0−3 °C for 24 h by anodizing an Al foil. The film was detached from the residual Al foil using the reversed-bias method at

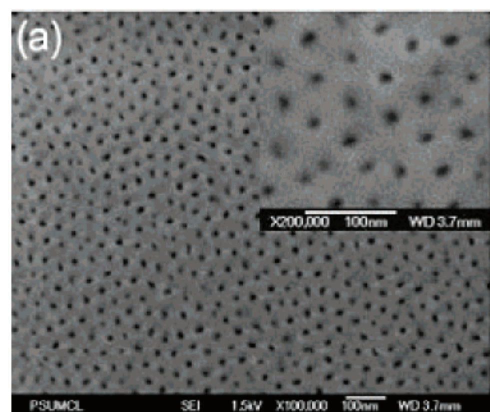

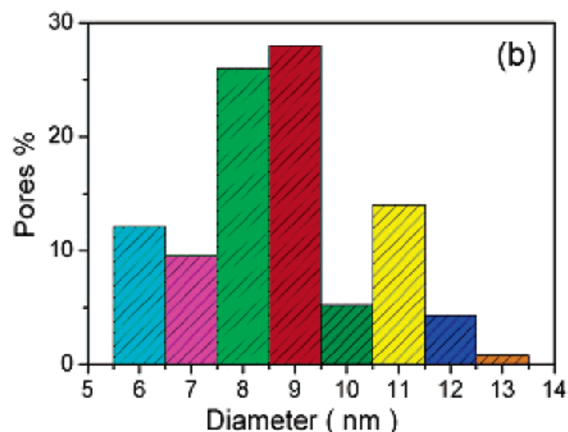

Figure 5. (a) FESEM image of AAO grown on an Al foil with 3 vol % H_2SO_4, anodized at 16 V and 0−3 °C after selective etching and detachment. The surface of the AAO was milled by an Ar ion beam for 10 min. (b) Plot of distribution of pore diameters determined from Figure 5a; 76% of the pores are below 10 nm in diameter.

−5 V for 5 min, and then a 0.5-μm-thick layer was removed from the bottom of the AAO film by milling the sample with a neutralized Ar ion beam. The sample was mounted on a liquid-nitrogen-cooled stage held at less than 90 K to avoid damaging the film during the milling process. The base pressure of the system was 1×10^{-6} Torr. Milling was done in a 0.5 mTorr Ar atmosphere. The accelerating voltage was 500 V. At an incidence angle of 54°, the beam intensity on the sample was 1.5−2.0 mA/cm^2. To detach the AAO film from Al foil, a relatively higher reversed-bias voltage, such as −5.0 V, was required. The higher reversed bias can produce more H_2 bubbles at the AAO/Al interfaces once the barrier layer is penetrated. Because the stress between the interface of AAO and the Al substrate is high, the H_2 bubbles at the bottom of the pores will promote the separation of the AAO film from the base Al foil with the tensile pressure of the gas.

Figure 5b shows the distribution of pore diameters of the AAO membrane shown in Figure 5a. Almost 76% of the pores have diameters of less than 10 nm, and 54% of them have pore sizes between 7.5 and 9.5 nm. Only 24% of the pores are larger than 10 nm but smaller than 14 nm. The pore density in Figure 5a reaches about 7×10^{10} pores/cm^2, but the pore distribution is less ordered with an average spacing of 20−30 nm between the pore channels.

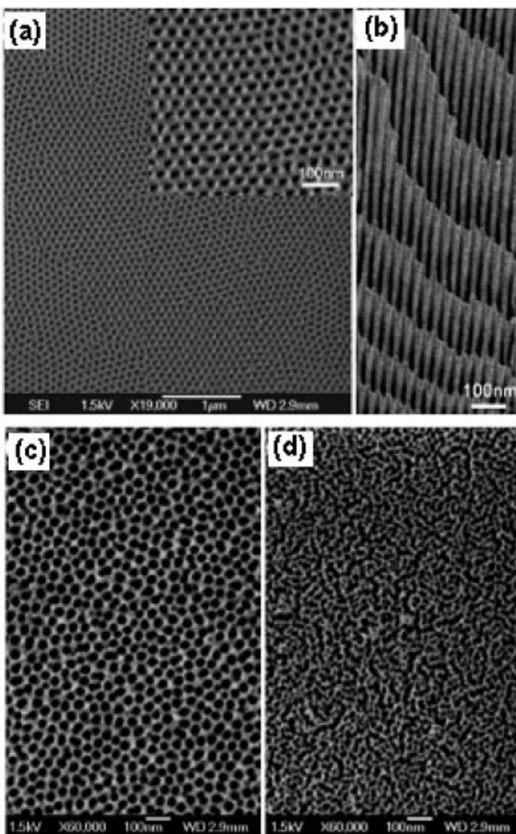

Figure 6. FESEM images of a free-standing AAO film anodized at −22 V and 0−3 °C from an Al foil and detached by the reversed-bias method. (a) Bottom surface after ion milling. (b) Cross-sectional image of the film. (c) Original top surface. (b) Original bottom surface.

In contrast to the irregular pore distribution of the small-pore membrane shown in Figure 5a, Figure 6a shows the FESEM image of the bottom surface of a free-standing AAO film, anodized at a relatively higher voltage of −22.0 V and 0−3 °C for 20 h and then separated from the residual Al foil under a reversed bias of − 5.0 V for 3 min. A 0.5-μm-thick bottom surface of the AAO film was removed by ion milling. The pore distribution shows perfectly hexagonal lattice structure over the entire AAO film, as checked by FESEM. The pore diameter is narrowly distributed and is around 22 ± 2 nm. Figure 5b is a cross-sectional view of the sample, showing regular and parallel channels. However, the pore distribution on both original surfaces of the AAO film before ion milling is random, as shown in Figure 6c (the top surface) and Figure 6d (the bottom surface). The pore size on the original surface looks slightly larger than that inside the membrane. This difference is partially from the effect of roughness of the original surface of the AAO film.

Electrodeposition of metallic nanowires into thick free-standing AAO films with pore diameters of less than 10 nm turned out to be very difficult because of the problem of wettibility. To achieve growth of nanowires, the bottom surface of the AAO film was ion milled at low temperature for 10 min. Then 30-nm-thick Cr and 200-nm-thick Ag films were thermally evaporated onto the milled surface at room temperature. Prior to electrodeposition, the AAO film with Ag/Cr electrode layers was wetted in *N*,*N*-dimethylformamide (DMF) for 30 min. During this period, the sample was softly ultrasonicated for 1 min to aid the wetting progress. The power of ultrasonication was carefully controlled because the ultrasonic waves may gradually peel off the Ag backing layer working as the cathode. We found that the Ar ion milling process is crucial for the deposition of nanowires into these free-standing sub-10 nm pore AAO films. This is because ion milling removes all of the residual barrier layer, opens each individual pore channel, and reduces the surface roughness, thereby enhancing the electrical contact in the electrodeposition process. It is relatively easier to immediately deposit Au into the wetted as-anodized AAO film on Ti/SiO_x/Si substrate after the completion of penetrating the oxide barrier layer by reverse bias.

Figure 7a shows a low-magnification TEM image of Au nanowires deposited at −2.5 V in small-pore AAO films shown in Figure 5. The inset is a selected-area electron diffraction (SAED) pattern on some of Au wire bundles. Fine structures of these wires were examined by HRTEM on a JEOL 2010 FETEM/STEM, as shown in Figure 7b and d, respectively. The diameter of the Au wire in Figure 7b is 7.2 nm, but the diameter of the wire can vary up to 25% along the length, as shown in the low-magnification TEM image of Figure 7c. Although 76% of the original pores in the AAO film of Figure 5 were shown to be less than 10 nm, most of the free-standing Au nanowires released from the AAO showed slightly larger diameters, ∼9−12 nm, as seen in Figure 7d, which is inconsistent with the results of the FESEM study. This disagreement may come from a number of reasons, namely, that (1) the filling factor of sub-10 nm pores is much lower than that of the larger-diameter pores, (2) most of the sub-10 nm diameter wires successfully grown into the pores were washed away or broken into small pieces during the preparation of nanowire suspension by using centrifugation and ultrasonic waves, or (3) the diameter of the original sub-10 nm wire increases after the wires were released from the AAO film because of a coarsening transformation toward lower free energy by “balling up” (i.e., by increasing in diameter while decreasing in length to reduce the total surface area). Previously, we have observed similar phenomena in other metallic nanowires. For example, in 40 nm Au−Sn heterojunction nanowires made from a polycarbonate template, the diameter of the low-melting-point Sn part in each Au−Sn wire is always larger than that of the Au segment.[30] For sub-10 nm Au wires, we have observed evidences of two individual wires grown into each other by surface atom diffusion (the details will be reported elsewhere). Even so, we do not exclude the possibility that the difference is from the low resolution of the FESEM.

It is worth noting that, after the anodization of Al foils at 16 V for 16−24 h, by totally dissolving the residual aluminum foil with saturated aqueous $HgCl_2$ and ion milling off the bottom layer we have also routinely obtained free-standing AAO films with sub-10 nm pores. However, compared to the reversed-bias method, the $HgCl_2$-etching approach has the disadvantages of longer processing time, loss of Al foil, and, especially, involvement of a toxic

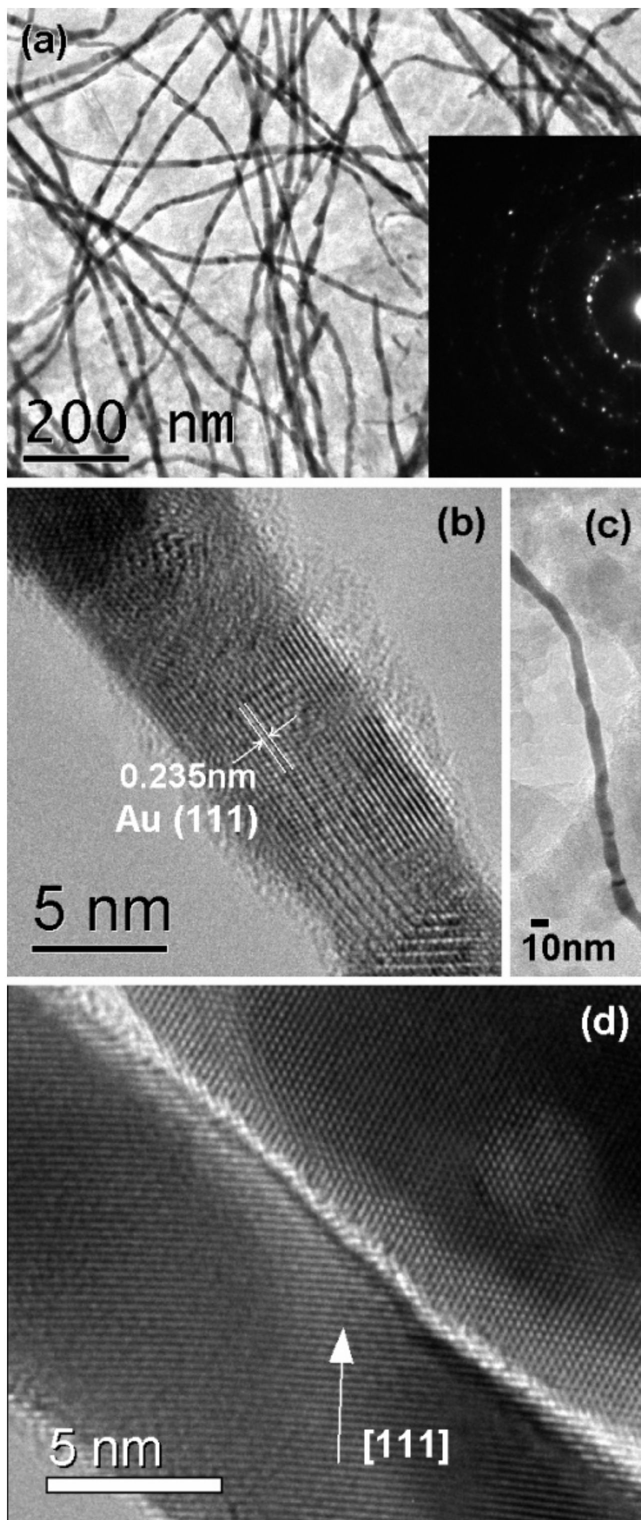

Figure 7. (a) Low-magnification TEM image of Au nanowire bundles and a SAED pattern. b and c, respectively, show HRTEM and low-magnification TEM images of a thin 7.2 nm Au wire. (d) HRTEM image of two selected Au wires of diameters 9−11 nm. All of the wires were made from the small-pore free-standing AAO membrane shown in Figure 5.

substance (Hg) and risk of contamination by the diffusion of Hg into the pore channels.

In summary, we have developed a simple method for penetrating the barrier layer of an AAO film and for detaching the AAO film from residual Al foil by reversing the bias voltage in situ after the anodization process is completed. Large pieces of free-standing AAO films with regular pore sizes below sub-10 nm were obtained. By combining this membrane preparation method with Ar ion milling and wetting enhancement processes, we have been able to deposit Au nanowires into the sub-10 nm pores of the AAO films. Further scaling down of the pore size and extension to the deposition of nanowires and nanotubes of materials other than Au should be possible by further optimizing this procedure.

Acknowledgment. We acknowledge fruitful discussions with Dr. Christine Keating and Mahy El-Kouedi. This work is supported by Penn State MRSEC funded by NSF under grant DMR-0213623 and partially supported by the Petroleum Research Fund (Q.L.).

References

(1) (a) Hulteen, J. C.; Martin, C. R. *J. Mater. Chem*. **1997**, *7*, 1075. (b) Martin, C. R. *Science* **1994**, *266*, 1961. (c) Martin C. R. *Chem. Mater*. **1996**, *8*, 1739. (d) Sapp, S. A.; Mitchell, D. T.; Martin, C. R. *Chem. Mater*. **1999**, *11*, 1183.
(2) (a) Nicewarner-Pena, S. R.; Freeman, R. G.; Reiss, B. D.; He, L.; Pena, D. J.; Walton, I. D.; Cromer, R.; Keating, C. D.; Natan, M. J. *Science* **2001**, *294*, 137. (b) Martin, B. R.; Dermody, D. J.; Reiss, B. D.; Fang, M.; Lyon, L. A.; Natan, M. J.; Mallouk, T. E. *Adv. Mater*. **1999**, *11*, 1021.
(3) Hong, B. H.; Bae, S. C.; Lee, C. W.; Jeong, S.; Kim, K. S. *Science* **2001**, *294*, 348.
(4) Liu, K.; Chien, C. L.; Searson, P. C.; Kui, Y. Z. *Appl. Phys. Lett*. **1998**, *73*, 1436.
(5) Tian, M. L.; Wang, J. G.; Kurtz, J. S.; Mallouk, T. E.; Chan, M. H. W. *Nano Lett*. **2003**, *3*, 919.
(6) Knez, M.; Bittner, A. M.; Boes, F.; Wege, C.; Jeske, H.; Maiss, E.; Kern, K. *Nano Lett*. **2003**, *3*, 1079.
(7) Wu, Y. Y.; Livneh, T.; Zhang, Y. X.; Cheng, G. S.; Wang, J. F.; Tang, J.; Moskovits, M.; Stucky, G. D. *Nano Lett*. **2004**, *4*, 2337.
(8) Rahman, S.; Yang, H. *Nano Lett*. **2003**, *3*, 439.
(9) Miao, Z.; Xu, D. S.; Ouyang, J. H.; Guo, G. L.; Zhao, X. S.; Tang, Y. Q. *Nano Lett.* **2002**, *2*, 717.
(10) Molares, M. E. T.; Buschmann, V.; Dobrev, D.; Neumann, R.; Scholz, R.; Schuchert, I. U.; Vetter, J. *Adv. Mater*. **2001**, *13*, 62.
(11) Nielsch, K.; Muller, F.; Li, A. P.; Gosele, U. *Adv. Mater*. **2000**, *12*, 582.
(12) Roy, E.; Fricoteaux, P.; Zhang, K. Y. *Nanosci. J. Nanotech*. **2001**, *1*, 323.
(13) Martin-Gonzalez, M.; Snyder, G. J.; Prieto, A. L.; Gronsky, R. G.; Sands, T.; Stacy, A. M. *Nano Lett.* **2003**, *3*, 973.
(14) Routkevitch, D.; Bigioni, T.; Moskovits, M.; Xu, J. M. *J. Phys. Chem*. **1996**, *100*, 14073.
(15) Yi, G.; Schwarzacher, W. *Appl. Phys. Lett*. **1999**, *74*, 1746.
(16) Tian, M. L.; Wang, J. G.; Snyder, J.; Kurtz, J. S.; Liu, Y.; Schiffer, P.; Mallouk, T. E.; Chan, M. H. W. *Appl. Phys. Lett*. **2003**, *83*, 1620.
(17) Iwasaki, T.; Motoi, T.; Den, T. *Appl. Phys*. **1999**, *75*, 2044.
(18) Nishizawa, M.; Menon, V. P.; Martin, C. R. *Science* **1995**, *268*, 700. (b) Wirtz, M.; Yu, S. F.; Martin, C. R. *Analyst* **2002**, *127*, 871.
(19) Xiao, Z. L.; Han, C. Y.; Welp, U.; Wang, H. H.; Kwok, W. K.; Willing, G. A.; Hiller, J. M.; Cook, R. E.; Miller, D. J.; Crabtree, G. W. *Nano Lett*. **2002**, *2*, 1293.
(20) Furneaux, R. C.; Rigby, W. R.; Davidson, A. P. *Nature* **1989**, *337*, 147.
(21) Masuda, H.; Hasegawa, F.; Ono, S. *J. Electrochem. Soc*. **1997**, *144*, L127.
(22) Asoh, H.; Nishio, K.; Nakao, M.; Tamamura, T.; Masuda, H. *J. Electrochem. Soc*. **2001**, *148*, B152.
(23) Toh, C. S.; M.Kayes, B.; Nemanick, E. J.; Lewis, N. S. *Nano Lett.* **2004**, *4*, 767.
(24) Heremans, J.; Thrush, C. M. *Phys. Rev. B* **1999**, *59*, 12579.
(25) Dresselhaus, M. S.; Lin, Y. M.; Rabin, O.; Dresselhaus, G. *Microscale Thermophys. Eng*. **2003**, *7*, 207.

(26) Jeong, S. H.; Hwang, H. Y.; Lee, K. H.; Jeong, Y. S. *Appl. Phys. Lett*. **2001**, 2052.
(27) Rabin, O.; Herz, P. R.; Lin, Y. M.; Akinwande, A. I.; Croniun, S. B.; Dresselhaus, M. S. *Adv. Funct. Mater.* **2003**, *13*, 631.
(28) Hu, W. C.; Gong, D. W.; Chen, Z.; Yuan, L. M.; Saito, K.; Grimes, C. A.; Kichambare, P. *Appl. Phys. Lett.* **2001**, *79*, 3083.
(29) Chen, G.; Delafuente, D. A.; Sarangapani, S.; Mallouk, T. E. *Catal. Today* **2001**, *67*, 341.
(30) Wang, J. G.; Tian, M. L.; Mallouk, T. E.; Chan, M. H. W. *Nano Lett.* **2004**, *4*, 1313.

NL0501112